Use of radial trajectories for motion correction in MRI

Internship Report

Delfín Calles Fantova
Université de Montpellier

June 2025
IMAG
Tutored by Franck Nicoud and Simon Mendez

Abstract

This internship report is meant to work as a beginner's introduction to the simulation of MRI and PC-MRI. More precisely to the use of radial trajectories for filling the k-space over the more traditional Cartesian ones when looking to reduce errors induced by motion. It presents the theory behind an MRI and the sequences that are used nowadays in medical imaging. Then there are some examples to illustrate how an MRI and a PC-MRI work. The first one is a more general example, to show how a normal MRI PC-MRI works and what are the normal results that should be expected. The second one is used to accentuate the relation between a sequence and the k-space and how we can choose either one to produce the other. The last one consists on an introduction of motion correction techniques that can be used in radial trajectories.

Contents

Chapter 1

Introduction

1.1 Motivation

Magnetic resonance imaging (MRI) is a non-invasive medical imaging technique used to generate pictures of the patient's anatomy and physiological processes inside the body. It was first presented by Paul Lauterbur [1] in 1973 and due to its importance in the medical imaging field, Paul Lauterbur and Peter Mansfield ended up receiving a Nobel Prize in medicine in 2003 for their works regarding MRI. Such an award going for a work that stems from other branches in Science than Medicine just showcases the importance of approaching MRI with techniques and ideas from other fields.
The way how IRM works consists in the use of magnetic fields in order to make certain protons in the body part of interest to emit a signal, which corresponds to the Fourier transform of the proton density and thus it will be contained in the reciprocal space known as k-space. This signal stored in the k-space will then be converted by an inverse Fourier transform to the image of the body part that we want to observe. In *Figure 1.1* there are two examples of the type of images that we can obtain when doing an MRI.
The way of filling this space has always been an interesting area of study, and the different ways a signal moves in the k-space when filling it are known as trajectories. Due to inherent properties that the k-space possesses, such as the ability of performing an inverse fast Fourier transform to the signal when it is collected in a Cartesian grid over the k-space, have made Cartesian trajectories the most used method in the clinic. It is a robust and well established method for which techniques have already been developed over

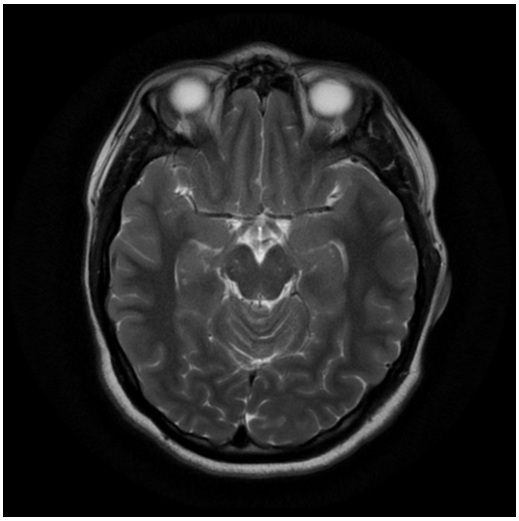

(a) *Normal appearance of a young person's brain. Case courtesy of Frank Gaillard, Radiopaedia.org, rID: 37605 [2]*

(b) *MRI showing the complete tear of the anterior cruciate ligament (ACL). Case courtesy of Lam Van Le, Radiopaedia.org, rID: 207562 [3]*

Figure 1.1: MRI examples.

the time to compensate for its shortcomings under certain circumstances. Despite that, the study of different sampling strategies remains open and work is still being done to find and study different methods that might work better than the usual Cartesian sampling for some cases [4]. From those techniques, the one that gets the most attention for its advantages over the classical method is the radial sampling [5]. Its robustness to motion induced artifacts in comparison to Cartesian sampling makes it already a better candidate when one cannot assure the patient to stay immobile (e.g. when performing an MRI to a child or a claustrophobic patient), or when the zone to be imaged is constantly moving (e.g. the lungs ot the heart).
Radial sampling has also been proved to be quite efficient when performing phase contrast magnetic resonance imaging (PC-MRI) [6] [7] [8], which refers to the techniques used while doing an MRI in order to determine flow velocities. It is usually done when the main objective is to study the blood flow and blood vessels, in *Figure 1.2* we can see some examples of PC-MRI.
During the thesis of Thomas Puiseux [11], the idea of performing an MRI to a simulation of the blood flow in a phantom came to light, known as *in silico* MRI. It was then developed during the thesis of Morgane Garreau [12].

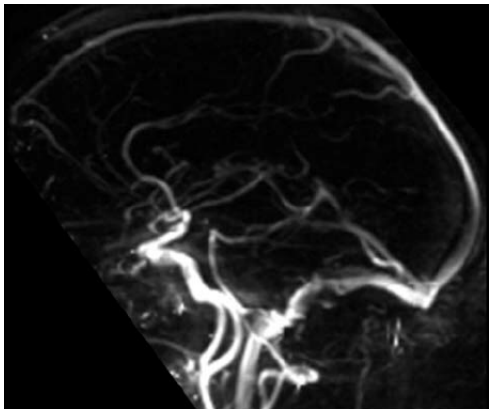

(a) *Three-dimensional PC-MRI of the intracranial vessels [9]*

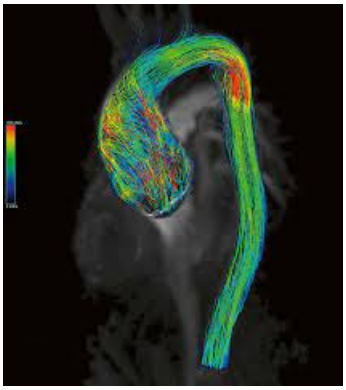

(b) *Hemodynamics of the aorta in a healthy patient, streamlines show a regular flow [10]*

Figure 1.2: Examples of figures obtained when performing a PC-MRI

To continue to improve this technique, the next step is to try to implement radial trajectories for the *in silico* MRI, to do so, a study of its advantages over more common techniques must be done.

1.2 Objectives and overview

1.2.1 Objectives

This document is the summary of the internship under the guidance of Franck Nicoud and Simon Mendez. The objective of the internship was to learn the fundamentals behind MRI and to understand the work that is being done here at IMAG on this subject to study how radial sampling techniques affect the *in silico* MRI that is being done here using the Yales2BIO solver [13] [14].

1.2.2 Overview

The second chapter is an introduction to the theory behind MRI, it presents the ideas behind an MRI and how it works. The same is done for PC-MRI. The third chapter presents the examples and the results obtained by running them on the Python solver that Morgane Garreau developed for her thesis

[12]. Firstly, there is an example in order to show how an MRI works. Secondly, the presentation of a method used to obtain sequences from a trajectory on the k-space, and how it is used to implement other sampling techniques directly. Finally, a presentation of motion correction techniques used in radial sampling and what are the results of using such techniques.
The fourth and final chapter analyzes and explain the results obtained. It also explains what are the main goals moving forward with the internship.

Chapter 2

MRI Theory

2.1 Physics background

2.1.1 The phenomenon of nuclear magnetic resonance

The idea of MRI relies on a phenomenon called nuclear magnetic resonance (NMR), which was first described by Isidor Rabi in 1938 [15]. It consists on the fact that atomic nucleus posses a non-zero nuclear spin when they are under the effect of an external magnetic field. It has many applications and it can be done with many different atoms, but for MRI, usually it is performed using the hydrogen atoms in the body.
The nuclear spin I is a quantum property of each nuclear species which in the presence of a magnetic field $\mathbf{B}_0$ gives rise to a magnetic moment $\boldsymbol{\mu}$ with an amplitude proportional to the nuclear spin. This magnetic moment precesses around the axis of the magnetic field at a frequency ω_0 known as the *Larmor frequency* that is proportional to the magnitude B_0 of the magnetic field $\mathbf{B}_0$, defined as:

$$\omega_0 = \gamma B_0$$

With γ being the gyromagnetic ratio, a constant characteristic of each isotope.
The equation describing the evolution of the magnetic moment along the time can be described as:

$$\frac{d\boldsymbol{\mu}}{dt} = \gamma \boldsymbol{\mu} \times \mathbf{B}_0 \tag{2.1}$$

Obviously, when performing an MRI more than one hydrogen atom is excited each time, so the study is done over a macroscopic magnetization $\mathbf{M}$ that is

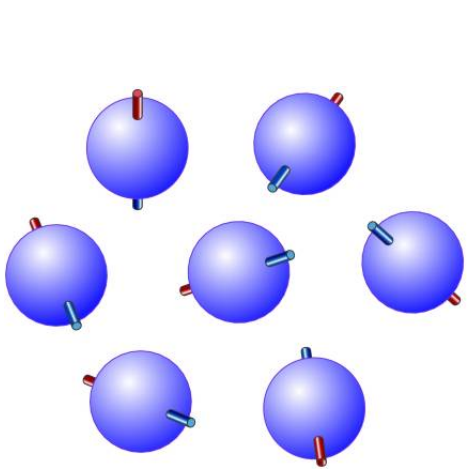

(a) *Spins under normal conditions, they move freely with no clear direction.*

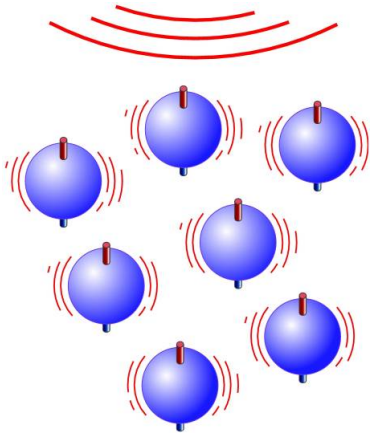

(b) *Once a strong magnetic field is applied, all the spins line up, the sum of all the lined up spins is what creates the magnetic vector.*

Figure 2.1: Scheme of the behavior of the magnetic spin under a strong magnetic field. [16]

defined as the sum of the magnetic moment of all the atoms N that found in a volume V. More precisely:

$$\mathbf{M} = \frac{1}{V}\sum_{i=1}^{N}\boldsymbol{\mu}_i \tag{2.2}$$

At thermal equilibrium, the magnetic vector $\mathbf{M}_0$ is defined as:

$$\mathbf{M} \approx \frac{\rho_0\gamma^2\hbar^2}{4kT}\mathbf{B}_0 \tag{2.3}$$

Where ρ_0 is the proton density per unit of volume, $\hbar$ is the reduced Planck constant, k is the Boltzmann constant and T is the temperature. *Figure 2.1* shows a simplified scheme that explains how the spins of the atoms behave when they are under a strong magnetic field.

2.1.2 NMR and Bloch equations

The principle of NMR relies on disrupting the precession movement of $\mathbf{M}$ around $\mathbf{B}_0$ by applying a temporary $\mathbf{B}_1(t)$ in the orthogonal plane. This

first step of disrupting the precession is called *excitation*. Once the $\mathbf{B}_1(t)$ is removed, $\mathbf{M}$ will begin to return to its original movement, this part is called *relaxation*. During the relaxation the NMR signal is measured.

Excitation

By convention, $\mathbf{B}_0$ is oriented along the z-axis, so $\mathbf{B}_0 = B_0\hat{e}_z$, with $\hat{e}_z$ being the vector of the canonical base $(\hat{e}_x, \hat{e}_y, \hat{e}_z)$ in $\mathbb{R}^3$, which is known as the fixed frame of reference. So the magnetic field $\mathbf{B}_1(t)$, by convention, occurs in the xy-plane and is oscillating.
Since $\mathbf{B}_1(t)$ oscillates, it appears natural that instead of working with the fixed laboratory frame of reference , a rotating frame of reference $(e'_x, e'_y, \hat{e}_z)$ is defined. $\mathbf{\Omega} = -\omega\hat{e}_z$ is the rotational angular velocity vector associated with the latter frame of reference. For any magnetic field $\mathbf{B}$, combining equations (2.1) and (2.2) gives [17]:

$$\begin{aligned} \frac{d\mathbf{M}}{dt} &= (\frac{d\mathbf{M}}{dt})' + \mathbf{\Omega} \times \mathbf{M} \\ \implies (\frac{d\mathbf{M}}{dt})' &= \frac{d\mathbf{M}}{dt} + \mathbf{M} \times \mathbf{\Omega} \\ &= \gamma\mathbf{M} \times \mathbf{B} + \mathbf{M} \times \mathbf{\Omega} \\ &= \gamma\mathbf{M} \times \mathbf{B_{eff}} \qquad \text{with } \mathbf{B_{eff}} = \mathbf{B} + \frac{\mathbf{\Omega}}{\gamma} \end{aligned} \tag{2.4}$$

In the rotating frame of reference associated with the frequency ω_0, $B_0\hat{e}_z = \frac{\omega_0}{\gamma}$ cancels out with $\frac{\mathbf{\Omega}}{\gamma}$, and $\mathbf{B_{eff}} = \mathbf{B}_1(t)$.
The oscillating magnetic field $\mathbf{B}_1$ applied during the excitation phase is called the radio-frequency pulse (RF-pulse). In the fixed laboratory frame, this field can be expressed as $\mathbf{B}_1(t) = B_1 cos(\omega_1 t)\hat{e}_x - B_1 sin(\omega_1 t)\hat{e}_y$. Where ω_1 indicates the precession frequency of the field B_1. In the rotating frame it is:

$$\begin{aligned} \begin{bmatrix} B_{1,x'}(t) \\ B_{1,y'}(t) \\ B_{1,\hat{z}}(t) \end{bmatrix} &= \begin{bmatrix} cos(\omega t) & -sin(\omega t) & 0 \\ sin(\omega t) & cos(\omega t) & 0 \\ 0 & 0 & 1 \end{bmatrix} \begin{bmatrix} B_1 cos(\omega_1 t) \\ -B_1 sin(\omega_1 t) \\ 0 \end{bmatrix} \\ &= \begin{bmatrix} B_1 cos((\omega - \omega_1)t) \\ B_1 sin((\omega - \omega_1)t) \\ 0 \end{bmatrix} \end{aligned} \tag{2.5}$$

To be able to tip the magnetization vector $\mathbf{M}$ the RF pulse has to be applied close to the *Larmor frequency*. If the on-resonance condition (e.g. $\omega = \omega_1 =$

ω_0), equation (2.5) reduces to $\mathbf{B}_1(t) = B_1 e'_x(t)$.
The angle of rotation α of the magnetization vector during the excitation is called the flip angle and is defined as $\alpha = \gamma \int_0^{t_{rf}} B_1(t)dt$, with t_{rf} indicating the duration of the RF-pulse.

Relaxation

Once the RF-pulse is finished, the relaxation phase begins. During this phase the magnetization vector starts to go back to its original position. This means that the component M_z of the vector $\mathbf{M}$, known as the longitudinal magnetization, grows again to its original value, while the M_x and M_y components, known as the transversal magnetization, start to disappear.

The Bloch equations

To study the evolution of the magnetization vector, Felich Bloch proposed a model in 1946 to describe the NMR phenomenon [18], for which he won a Nobel prize in Physics in 1952. He introduced two constants T_1 and T_2 which represents the growth of the longitudinal magnetization and the decay of the transverse magnetization, respectively. These constants depend on the tissues and were obtained experimentally. The Bloch equations, in the fixed laboratory frame are described as:

$$\frac{d\mathbf{M}(t)}{dt} = \gamma \mathbf{M}(t) \times \mathbf{B}(t) + \frac{1}{T_1}(M_0 - M_z(t))\hat{e}_z - \frac{1}{T_2}(M_x(t)\hat{e}_x + M_y(t)\hat{e}_y) \quad (2.6)$$

Where M_0 refers to the magnitude of the longitudinal magnetization when in thermal equilibrium.
In the rotating frame, using (2.4) gives:

$$\frac{d\mathbf{M}(t)}{dt} = \gamma \mathbf{M}(t) \times \mathbf{B_{eff}}(t) + \frac{1}{T_1}(M_0 - M_z(t))\hat{e}_z - \frac{1}{T_2}(M'_x(t)e'_x + M'_y(t)e'_y) \quad (2.7)$$

In the rotating frame , the expressions of $\mathbf{M}(t)$ and $\mathbf{B_{eff}}(t)$ are:

$$\begin{aligned} \mathbf{M}(t) &= M'_x(t)e'_x + M'_y(t)e'_y + M_z(t)\hat{e}_z \\ \mathbf{B_{eff}}(t) &= \mathbf{B}_0 + \mathbf{B}_1(t) + \frac{\mathbf{\Omega}}{\gamma} \\ &= B_1 cos((\omega - \omega_1)t)e'_x + B_1 sin((\omega - \omega_1)t)e'_y + (B_0 - \frac{\omega}{\gamma})\hat{e}_z \end{aligned}$$

Assuming that the on-resonance condition is met, the Bloch equations in the rotating frame of reference (2.6), when written in matrix form, become:

$$\frac{d}{dt}\begin{bmatrix} M'_x(t) \\ M'_y(t) \\ M_z(t) \end{bmatrix} = \begin{bmatrix} -\frac{1}{T_2} & 0 & 0 \\ 0 & -\frac{1}{T_2} & \gamma B_1(t) \\ 0 & -\gamma B_1(t) & -\frac{1}{T_1} \end{bmatrix} \begin{bmatrix} M'_x(t) \\ M'_y(t) \\ M_z(t) \end{bmatrix} + \begin{bmatrix} 0 \\ 0 \\ \frac{M_0}{T_1} \end{bmatrix} \tag{2.8}$$

Analytical solution for the excitation

Since the RF-pulse is of short duration, $\omega_1 >> \frac{1}{T_1}, \frac{1}{T_2}$ is assumed. Which means that the relaxation effects of the Bloch equations during the excitation can be ignored, so equation (2.8) becomes:

$$\frac{d}{dt}\begin{bmatrix} M'_x(t) \\ M'_y(t) \\ M_z(t) \end{bmatrix} = \begin{bmatrix} 0 & 0 & 0 \\ 0 & 0 & \gamma B_1 \\ 0 & -\gamma B_1 & 0 \end{bmatrix} \begin{bmatrix} M'_x(t) \\ M'_y(t) \\ M_z(t) \end{bmatrix} \tag{2.9}$$

Declaring $\mathbf{M}_0 = (0, 0, M_0)^T$ as its initial conditions we find ourselves with a system of differential equations which we can solve, getting as solution:

$$\begin{cases} M'_x(t) = 0 \\ M'_y(t) = M_0 sin(\alpha) \\ M_z(t) = M_0 cos(\alpha) \end{cases} \tag{2.10}$$

With α being the flip angle. In *Figure 2.2* we can observe the evolution of the magnetization vector during the excitation phase.

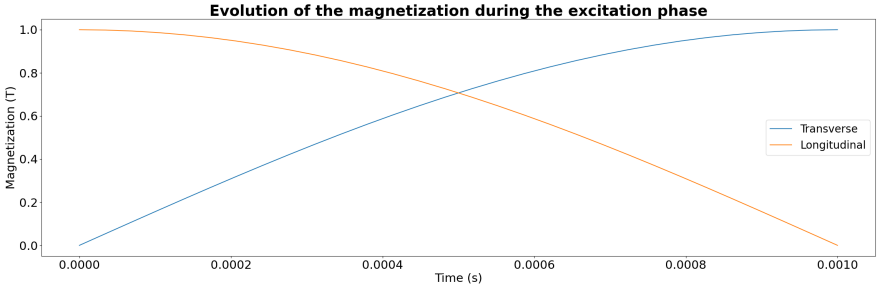

Figure 2.2: *Evolution of the transversal and magnetization vectors during the excitation phase for a flip angle of 90º*

Analytical solution for the relaxation

As we have already stated, the relaxation phase begins when the $\mathbf{B}_1$ goes back to zero, so then equation (2.8) becomes:

$$\frac{d}{dt}\begin{bmatrix} M'_x(t) \\ M'_y(t) \\ M_z(t) \end{bmatrix} = \begin{bmatrix} -\frac{1}{T_2} & 0 & 0 \\ 0 & -\frac{1}{T_2} & 0 \\ 0 & 0 & -\frac{1}{T_1} \end{bmatrix} \begin{bmatrix} M'_x(t) \\ M'_y(t) \\ M_z(t) \end{bmatrix} + \begin{bmatrix} 0 \\ 0 \\ \frac{M_0}{T_1} \end{bmatrix} \tag{2.11}$$

To solve this differential equation, it is separated in the components of the longitudinal and transversal magnetization. For that the complex representation of the transverse magnetization is introduced: $M'_{xy}(t) = M'_x(t) + iM'_y(t) =\mid M_{xy}(t) \mid e^{i\phi(t)}$, where $\mid M_{xy}(t) \mid$ is the modulus of the transverse magnetization and $\phi(t)$ indicates its angle, known as phase. As before, the solution of the system of ordinary differential equation has its solutions defined as:

$$\begin{cases} M'_{xy}(t) = M'_{xy}(t_0)e^{-\frac{t-t_0}{T2}} \\ M_z(t) = (M_z(t_0) - M_0)e^{-\frac{t-t_0}{T2}} + M_0 \end{cases} \tag{2.12}$$

Where $t_0 \geq t_{rf}$ indicates the end of the excitation phase. Since the transverse magnetization is a complex number, the change to the fixed laboratory frame is immediate, just multiply the transverse magnetization by $e^{-i\omega_0 t}$, obtaining:

$$\begin{cases} M'_{xy}(t) = M'_{xy}(t_0)e^{i\omega_0 t}e^{-\frac{t-t_0}{T2}} =\mid M_{xy}(t_0) \mid e^{-i(\omega_0 t - \phi(t_0))}e^{-\frac{t-t_0}{T2}} \\ M_z(t) = (M_z(t_0) - M_0)e^{-\frac{t-t_0}{T2}} + M_0 \end{cases} \tag{2.13}$$

As before, *Figure 2.3* shows the evolution of the magnetization vector during the relaxation phase.

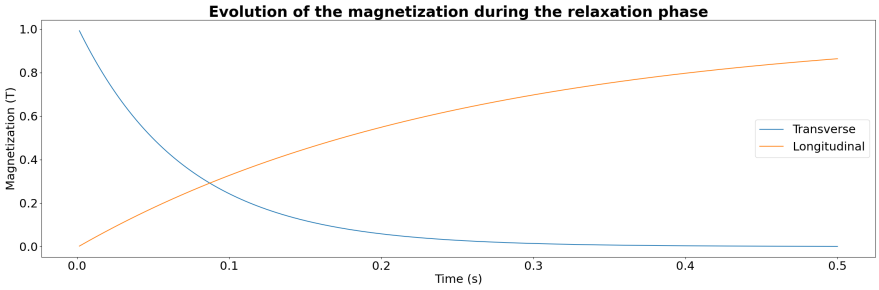

Figure 2.3: *Evolution of the transversal and magnetization vectors during the relaxation phase for a flip angle of 90^o in the rotating frame. The T_1 and T_2 parameter are 250 and 70 ms respectively, they correspond to the times for fat tissue. $t_0 = 1ms$ and $TR = 500ms$, which is the average duration of a TR in T1-weighted imaging.*

2.1.3 NMR signal

There are many ways to work and interact with the NMR signal when doing an MRI [17]. Here, the most basic ones are introduced.

Free Induction Decay (FID)

The most basic MRI experiment, only an RF-pulse is applied in order to start the excitation phase and then the relaxation phase occurs. Since the signal $s(t)$ is proportional to the electromotive force, it is:

$$s(t) \propto -\frac{d}{dt}\iiint_V (M_x(\mathbf{r},t)\mathcal{B}_x^r(\mathbf{r}) + M_y(\mathbf{r},t)\mathcal{B}_y^r(\mathbf{r}) + M_z(\mathbf{r},t)\mathcal{B}_z^r(\mathbf{r})d^3r \quad (2.14)$$

Where $\boldsymbol{\mathcal{B}}^r(\mathbf{r}) = (\mathcal{B}_x^r(\mathbf{r}), \mathcal{B}_y^r(\mathbf{r}), \mathcal{B}_z^r(\mathbf{r}))^T$ indicates the magnetic field per unit current that would be produced by the receiver coil (part of the MRI machine that takes part in the signal detection) at the location $\mathbf{r}$.
From (2.13) is derived:

$$\frac{dM_{xy}}{dt} = -(i\omega_0 + \frac{1}{T_2}) \mid M_{xy}(\mathbf{r},t_0) \mid e^{-i(\omega_0 t - \phi(\mathbf{r},t_0))}e^{-\frac{t-t_0}{T2}}$$
$$\frac{dM_z}{dt} = -\frac{1}{T_1}(M_z(\mathbf{r},t_0) - M_0)e^{-\frac{t-t_0}{T_1}}$$

As before, working under the assumption that $\omega_0 >> \frac{1}{T_1}, \frac{1}{T_2}$, the longitudinal magnetization can be neglected and the transverse magnetization approximated as:

$$\begin{cases} \frac{dM_x}{dt} & \approx -\omega_0 \mid M_{xy}(\mathbf{r}, t_0) \mid sin(\omega_0 t - \phi(\mathbf{r}, t_0)) e^{-\frac{t-t_0}{T_2}} \\ \frac{dM_y}{dt} & \approx -\omega_0 \mid M_{xy}(\mathbf{r}, t_0) \mid cos(\omega_0 t - \phi(\mathbf{r}, t_0)) e^{-\frac{t-t_0}{T_2}} \end{cases} \tag{2.15}$$

So then (2.14) becomes:

$$\begin{aligned} s(t) \propto \omega_0 \iiint_V e^{-\frac{t-t_0}{T_2}} \mid M_{xy}(\mathbf{r}, t_0) \mid & (sin(\omega_0 t - \phi(\mathbf{r}, t_0)) \mathcal{B}_x^r(\mathbf{r}) \\ & + cos(\omega_0 t - \phi(\mathbf{r}, t_0)) \mathcal{B}_y^r(\mathbf{r})) d^3 r \end{aligned} \tag{2.16}$$

Which can be simplified further by introducing the complex notation of the transverse sensitivity of the receiver coil, obtaining:

$$\begin{aligned} s(t) \propto \omega_0 \iiint_V e^{-\frac{t-t_0}{T_2}} \mid M_{xy}(\mathbf{r}, t_0) \mid\mid \mathcal{B}_{xy}^r(\mathbf{r}) \mid & sin(\omega_0 t + \theta_{\mathcal{B}^r}(\mathbf{r}) \\ & - \phi(\mathbf{r}, t_0)) d^3 r \end{aligned} \tag{2.17}$$

The signal as it is right now is dominated by the rapid oscillations of the *Larmor frequency* ω_0 inside the sinusoidal term. In order to eliminate those oscillations the signal passes through an additional step called *demodulation*. This step results in viewing the signal from the rotating frame of reference instead.

To do that the signal is multiplied by $sin(\omega_0 t)$ one first time and then a second time by $-cos(\omega_0 t)$, creating two channels, the real channel and the imaginary channel, respectively.

Since the procedure for both is the same, here only the work on the imaginary channel is showed. It is quite straightforward, it uses the trigonometric identity $cos(a)sin(b) = \frac{1}{2}(sin(a+b) - sin(a-b))$ with $a = \omega_0 t$ and $b = \omega_0 t + \theta_{\mathcal{B}^r}(\mathbf{r}) - \phi(\mathbf{r}, t_0)$, getting:

$$\begin{aligned} -cos(\omega_0 t) sin(\omega_0 t + \theta_{\mathcal{B}^r}(\mathbf{r}) - \phi(\mathbf{r}, t_0)) = \frac{1}{2} (& sin(\phi(\mathbf{r}, t_0) - \theta_{\mathcal{B}^r}(\mathbf{r})) \\ & - sin(2\omega_0 t + \theta_{\mathcal{B}^r}(\mathbf{r}) - \phi(\mathbf{r}, t_0))) \end{aligned}$$

There still is a high-frequency sinusoidal term there, but it is removed by applying a low pass filtering. The demodulated and low pass filtered imaginary

channel s_{im} is defined as:

$$s_{im}(t) \propto \omega_0 \iiint_V e^{-\frac{t-t_0}{T_2}} \mid M_{xy}(\mathbf{r}, t_0) \mid\mid \mathcal{B}^r_{xy}(\mathbf{r}) \mid \Im(e^{i(\phi(\mathbf{r},t_0)-\theta_{\mathcal{B}^r}(\mathbf{r}))})d^3r$$

The same goes for the real channel s_{re}:

$$s_{re}(t) \propto \omega_0 \iiint_V e^{-\frac{t-t_0}{T_2}} \mid M_{xy}(\mathbf{r}, t_0) \mid\mid \mathcal{B}^r_{xy}(\mathbf{r}) \mid \Re(e^{i(\phi(\mathbf{r},t_0)-\theta_{\mathcal{B}^r}(\mathbf{r}))})d^3r$$

So the signal collected by the receiver coil at the end is a complex signal $S(t) = s_{re}(t) + s_{im}(t)$ defined as:

$$\begin{aligned} S(t) &\propto \omega_0 \iiint_V e^{-\frac{t-t_0}{T_2}} \mid M_{xy}(\mathbf{r}, t_0) \mid\mid \mathcal{B}^r_{xy}(\mathbf{r}) \mid e^{i(\phi(\mathbf{r},t_0)-\theta_{\mathcal{B}^r}(\mathbf{r}))}d^3r \\ &\propto \omega_0 \iiint_V M'_{xy}(\mathbf{r}, t)\boldsymbol{\mathcal{B}}^*_{xy}(\mathbf{r})d^3r \end{aligned} \tag{2.18}$$

Where $\boldsymbol{\mathcal{B}}^*_{xy}(\mathbf{r}) =\mid \mathcal{B}^r_{xy}(\mathbf{r}) \mid e^{-i\theta_{\mathcal{B}^r}(\mathbf{r})}$ is the complex conjugate of $\boldsymbol{\mathcal{B}}_{xy}(\mathbf{r})$.

Adding spatial-temporal dependencies to the precession frequency

Up until this point only ideal conditions have been considered, which works great as a way to introduce the theory, although it might not be suited for all the inexactitudes that might appear when performing an MRI. One of the problems to address here is the appearance of spatial-temporal dependencies due to inhomogeneities in the magnetic field. Implying that an isochromat (which is a group of atoms that has the same precession frequency) is not precessing at the *Larmor frequency* but:

$$\omega(\mathbf{r}, t) = \omega_0 + \gamma B_z(\mathbf{r}, t) = \omega_0 + \Delta\omega(\mathbf{r}, t)$$

By definition, the phase of the transverse magnetization in the fixed laboratory frame is:

$$\phi(\mathbf{r}, t) = \phi(\mathbf{r}, t_0) - \omega_0(t - t_0) - \int_{t_0}^{t} \Delta\omega(\mathbf{r}, t')dt'$$

When passed to the rotating frame, the term $\omega_0(t - t_0)$ vanishes and we get:

$$\phi(\mathbf{r}, t) = \phi(\mathbf{r}, t_0) - \int_{t_0}^{t} \Delta\omega(\mathbf{r}, t')dt'$$

When taking into account the spatial-temporal dependencies of $\omega(\mathbf{r},t)$ instead of (2.18) we get:

$$S(t) \propto \iiint_V \omega(\mathbf{r},t) e^{-\frac{t-t_0}{T_2}} \mid M_{xy}(\mathbf{r},t_0) \mid\mid \mathcal{B}^r_{xy}(\mathbf{r}) \mid \cdot \\ \cdot\, e^{i(\phi(\mathbf{r},t_0) - \int_{t_0}^{t} \Delta\omega(\mathbf{r},t')dt' - \theta_{\mathcal{B}^r}(\mathbf{r}))} d^3r \tag{2.19}$$

It is assumed that $\omega(\mathbf{r},t)$ is largely dominated by ω_0 so it can still be taken from the integral, and by adding a constant Λ to represent the gain factors due to the electronic detection system, the signal is then expressed as:

$$S(t) \propto \omega_0 \Lambda \iiint_V e^{-\frac{t-t_0}{T_2}} \mid M_{xy}(\mathbf{r},t_0) \mid\mid \mathcal{B}^r_{xy}(\mathbf{r}) \mid \cdot \\ \cdot\, e^{i(\phi(\mathbf{r},t_0) - \int_{t_0}^{t} \Delta\omega(\mathbf{r},t')dt' - \theta_{\mathcal{B}^r}(\mathbf{r}))} d^3r \tag{2.20}$$

The signal can be represented not as being proportional to the magnetization $\mathbf{M}$ but as being proportional to the proton spin density. First of all, the transverse magnetization is rewritten as a function of the proton spin density. To do that equations (2.3) and (2.10) are combined to obtain:

$$\mid M_{xy}(\mathbf{r},t_0) \mid = M_0(\mathbf{r}) sin(\alpha) = \rho_0(\mathbf{r}) \frac{\gamma^2\hbar^2}{4kT} sin(\alpha) B_0$$

The complex signal becomes:

$$S(t) \propto \iiint_V e^{-\frac{t-t_0}{T_2}} \rho(\mathbf{r}) e^{i\phi(\mathbf{r},t)} = \iiint_V \rho(\mathbf{r},T_2) e^{i\phi(\mathbf{r},t)} d^3r \tag{2.21}$$

Where $\rho(\mathbf{r},T_2) = e^{-\frac{t-t_0}{T_2}} \rho(\mathbf{r}) = e^{-\frac{t-t_0}{T_2}} \omega_0 \Lambda \rho_0(\mathbf{r}) \frac{\gamma^2\hbar^2}{4kT} sin(\alpha) B_0 \boldsymbol{\mathcal{B}}^*_{xy}(\mathbf{r})$ is the effective spin density.

One of the main issues when performing a Free Induction Decay experiment for MRI, is that there is no way to know where the signal is coming from and thus it is impossible to reconstruct an image. More complex signal sequences, like the one presented later in this section present a solution to this problem.

Gradient Echo (GRE)

A GRE sequence relies on the use of spatially linearly varying fields, known as gradients, after the application of a unique RF-pulse. The gradient $\mathbf{G}(t)$

is defined as:

$$\mathbf{G}(t) = G_x(t)\hat{e}_x + G_y(t)\hat{e}_y + G_z(t)\hat{e}_z = \frac{\partial B_z}{\partial x}(t)\hat{e}_x + \frac{\partial B_z}{\partial y}(t)\hat{e}_y + \frac{\partial B_z}{\partial z}(t)\hat{e}_z$$

After the RF-pulse, when accounting for this gradient, the precession frequency becomes:

$$\omega(\mathbf{r}, t) = \omega_0 + \gamma \mathbf{G}(t) \cdot \mathbf{r}$$

And the phase in the rotating frame of reference is written as:

$$\phi(\mathbf{r}, t) = \phi(\mathbf{r}, t_0) - \gamma \int_{t_0}^{t} \mathbf{G}(t') \cdot \mathbf{r} dt'$$

To understand how gradients can be used to spatially localize the signal an explanation on how to construct a basic 3D GRE sequence is done, starting from a 1D GRE sequence and developing from there. In *Figure 2.4* there is a comparison between what to spatially encoding a signal means in terms of coloring the voxels of a cube.

1) **1D: Frequency-encoding:**
   In 1D, which by convention, is done over the x-direction, the simplest GRE sequence is composed of a single RF-pulse followed by 2 lobes of opposite strength G_x, which localize the signal in one dimension. To simplify and without loss of generality, the relaxation effects caused by $e^{-\frac{t-t_0}{T_2}}$ can be ignored. Then in 1D, modifying the 3D signal expression (2.21) means:

   $$S(t) = \int \rho(x) e^{i\phi(x,t)} dx$$

   Where $\rho(x) = \int\int \rho(\mathbf{r}) dz dy$ represents the effective spin density.
   When the expression of the phase with the gradient is included:

   $$S(t) = \int \rho(x) e^{i\int_0^t (-\gamma x G_x(t'))dt'} dx = \int \rho(x) e^{-i\gamma x \int_0^t G_x(t')dt'} dx \qquad (2.22)$$

   It can be observed that the expression of the signal in (2.22) is quite similar to a Fourier transform, which can be achieved more clearly once the time-dependent spatial frequency $k_x(t) = \frac{\gamma}{2\pi}\int_0^t G_x(t')dt'$ are introduced[19] [20]. With this, it is pretty clear that the signal $S(k_x)$

and the spin density $\rho(x)$ can be defined as a Fourier pair:

$$S(k_x) = \hat{\rho}(k_x) = \int \rho(x) e^{-i2\pi k_x x} dx$$
$$\rho(x) = \tilde{S}(x) = \int S(k_x) e^{i2\pi k_x x} dk_x$$

Right now it is assumed that the signal is collected continuously, which is never the case, a more appropriate description is to consider a signal being sampled in a finite number of spatial frequencies during a determined amount of time. Which mathematically gives the measured signal s_m as:

$$s_m(k_x) = \Delta k_x \sum_{p=0}^{N-1} S(p\Delta k_x)\delta(k_x - p\Delta k_x)$$

Where Δk_x represents the spacing between spatial frequencies. So the reconstructed image ρ_r that comes from the measured signal is:

$$\rho_r(x) = \tilde{s}_m(x) = \Delta k_x \sum_{p=0}^{N-1} S(p\Delta k_x) e^{i2\pi p \Delta k_x x}$$

Since it still is a Fourier pair, the inverse path can also be done, obtaining:

$$\rho_r(x) = \Delta x \sum_{q=0}^{N-1} \rho(q\Delta x)\delta(x - q\Delta x)$$
$$s_m(k_x) = \hat{\rho}_m(k_x) = \Delta x \sum_{q=0}^{N-1} \rho(q\Delta x) e^{-i2\pi q \Delta x k_x}$$

In the definitions, the signal is collected by moving forward along the spatial frequency k_x direction, hence why this type of encoding is called frequency encoding.

2) **2D: Phase-encoding**
This is quite straightforward, a spatial frequency $k_y(t)$ associated to the y direction like in the 1D case is defined as $k_y(t) = \frac{\gamma}{2\pi} \int_0^t G_y(t')dt'$.

Despite working with a 2D signal now, the steps are the same as in the 1D case, giving:

$$\rho_r(q_x\Delta x, q_y\Delta y) = \Delta k_x \Delta k_y \sum_{p_x=0}^{N_x-1}\sum_{p_y=0}^{N_y-1} s_m(p_x\Delta k_x, p_y\Delta k_y) e^{-i2\pi(q_x\Delta x p_x\Delta k_x + q_y\Delta y p_y \Delta k_y)}$$

$$s_m(p_x\Delta k_x, p_y\Delta k_y) = \Delta x \Delta y \sum_{q_x=0}^{N_x-1}\sum_{q_y=0}^{N_y-1} \rho_r(q_x\Delta x, q_y\Delta y) e^{-i2\pi(q_x\Delta x p_x\Delta k_x + q_y\Delta y p_y \Delta k_y)}$$

The usual method to fill the k-space (which is the space of our spatial coordinates) is the Cartesian raster-like trajectory, which consist of firstly move along the k_y direction to then collect the signal from all the k_x that are on that line. The name phase-encoding comes from the fact that once the G_y gradient is played in order to get to the k_y of interest, each isochromat experiences a dephasing in respect to the others depending on their position on the y-direction.

3) **3D: Volume imaging** The most common approach is to perform a second phase-encoding gradient $G_z(t)$ along the z-direction, to do so the spatial frequency alongside the z-direction $k_z(t) = \frac{\gamma}{2\pi}\int_0^t G_z(t')dt'$ is defined.

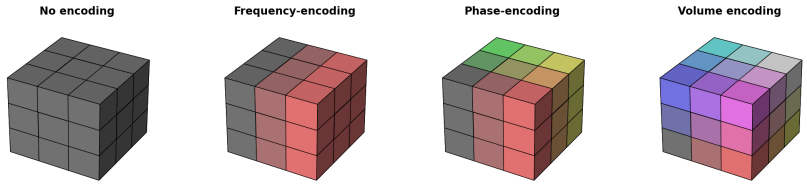

Figure 2.4: *Scheme to explain how to spatially encode a signal in 3D. From left to right it shows all the processes that are being done to fully encode the signal received from a 3D object. Spatially encoding is represented by changing the color of the voxel, meaning that the voxels sharing the same color, also share the same signal. At the end, each voxel should have a unique color.*

2.2 Phase-contrast imaging

Phase-contrast imaging (PC-MRI) is a medical imaging technique that aims to quantify the blood velocity. As its name suggest the idea behind this technique relies on the usage of the additional phase shift that is caused by the moving isochromats (e.g. blood). To understand the basics of this method, look the expression of the phase at the position $\mathbf{r}$ at echo time T_E (which is the time where the signal achieves its maximum amplitude during the readout):

$$\phi(\mathbf{r}, T_E) = \phi_0 - \gamma \int_0^{T_E} \mathbf{G}(t) \cdot \mathbf{r}(t) dt \tag{2.23}$$

With ϕ_0 being a background phase that depends on the additional phase and the field inhomogeneities. Since the particles are now moving, the position $\mathbf{r}(t)$ of an isochromat at an arbitrary time instant t_{exp} can be expanded with a Taylor series:

$$\mathbf{r}(t) = \sum_{n=0}^{\infty} \frac{\mathbf{r}^{(n)}(t_{exp})}{n!}(t - t_{exp})$$

Inserting this expansion to the expression of the phase gives:

$$\begin{aligned}
\phi(\mathbf{r}, T_E) =& \phi_0 - \gamma \mathbf{r}(t_{exp}) \cdot \int_0^{T_E} \mathbf{G}(t) dt - \gamma \mathbf{u}(t_{exp}) \cdot \int_0^{T_E} \mathbf{G}(t)(t - t_{exp}) dt \\
&- \gamma \frac{\mathbf{a}(t_{exp})}{2} \cdot \int_0^{T_E} \mathbf{G}(t)(t - t_{exp})^2 dt - ... \\
&= \phi_0 - \gamma \mathbf{r}(t_{exp}) \cdot \mathcal{M}_0 - \gamma \mathbf{u}(t_{exp}) \cdot \mathcal{M}_1 \\
&- \gamma \frac{\mathbf{a}(t_{exp})}{2} \cdot \mathcal{M}_2 - ...
\end{aligned}$$

Where $\mathbf{u}(t_{exp}) = (u(t_{exp}), v(t_{exp}), w(t_{exp}))^T = \mathbf{r}'(t_{exp})$, $\mathbf{a}(t_{exp}) = \mathbf{r}''(t_{exp})$ and $\mathcal{M}_n = \int_0^{T_E} \mathbf{G}(t)(t - t_{exp})^n dt$, denote the velocity, acceleration and n-th gradient moment, respectively.

When performing PC-MRI, a practical assumption to make is that the velocity is constant during a repetition time T_R (which is the time that it takes to complete a single pulse sequence), so that means $\mathbf{u} = (u, v, w)^T$ and $\mathbf{a} = (0, 0, 0)^T$.

The GRE pulse sequence described in *Section 2.1.3* can be adapted with more gradients to perform a PC-MRI. The most usual gradients forms used to perform this are bipolar gradients, which are two lobes of inverse polarity

but same duration, and they are played in the same direction of the velocity we want to find. With this gradient, $\mathcal{M}_0$ is cancelled and only the background phase ϕ_0 and $\mathcal{M}_1$ remains.
Since the background phase is still there and only the factor that contains the velocity is needed, another measurement has to be taken. It usually is the same sequence with the bipolar gradient inverted, but any sequence that can eliminate the background phase from the previous one works.
To demonstrate how a PC-MRI works, two measurements to find the velocity u along the x-axis have been taken. The first one $\phi_b(\mathbf{r}, T_E) = \phi_0 - \gamma u \mathcal{M}_1$ was the one where a bipolar gradient was applied, and the second one $\phi_{fc}(\mathbf{r}, T_E) = \phi_0$ is the one where a flow compensating gradient was used. Then the difference between phases (hence why it is called phase-contrast) is calculated to find an expression of u:

$$\Delta\phi(\mathbf{r}, T_E) = \phi_{fc}(\mathbf{r}, T_E) - \phi_b(\mathbf{r}, T_E) = \gamma u \Delta\mathcal{M}_1$$

With $\Delta\mathcal{M}_1$ being a general way to indicate the difference between the first order moments of both phases, although in this precise case it would only be consisting of the moment in the phase containing the bipolar gradient. It follows immediately that:

$$u = \frac{\Delta\phi(\mathbf{r}, T_E)}{\gamma\Delta\mathcal{M}_1} \tag{2.24}$$

The phase is simply the argument of the complex transverse magnetization, so it is defined between the interval $[-\pi, \pi]$, and so is the phase difference $\Delta\phi(\mathbf{r}, t)$. That means that the GRE sequence must be constructed so that when performing a PC-MRI, the maximal velocity results in a phase difference of π. To do so a user-defined parameter called velocity sensitivity or velocity encoding which requires an *a priori* knowledge of the expected flow is defined as:

$$u_{enc} = \frac{\pi}{\gamma\Delta\mathcal{M}_1}$$

This parameter of velocity encoding can be defined in any direction, so the velocity can be reconstructed in any direction just by creating the right sequence. At the end, by defining the velocity encoding for all three directions

as $V_{ENC} = (u_{enc}, v_{enc}, w_{enc})^T$, the velocity is reconstructed with the formula:

$$\begin{aligned} u &= \frac{u_{enc}}{\pi}\Delta\phi_x(\mathbf{r}, T_E) \\ v &= \frac{v_{enc}}{\pi}\Delta\phi_y(\mathbf{r}, T_E) \\ w &= \frac{w_{enc}}{\pi}\Delta\phi_z(\mathbf{r}, T_E) \end{aligned} \tag{2.25}$$

Chapter 3

Testing and manipulating MRI sequences

3.1 Introduction

This chapter contains some simple examples to illustrate the theory that has been presented in the previous chapter, which correspond to the first test-case alongside the work that has been done to study how different trajectories might be used when doing an MRI in order to solve some of the problems that might appear when using the classical methods. This corresponds to the reconstruction of GRE sequences from trajectories, so there is a quick way of testing new trajectories and its properties without the need to directly implement them in the code. It also presents an alternative to Cartesian trajectories with the use of radial trajectories for the correction of motion artifacts when doing an MRI.

3.2 Python solver example

This is a simple example in order to briefly explain how an MRI works and what can be expected.
This example uses the Python solver that Morgane Garreau developed during her thesis [12]. Inside this solver there are implemented the basic functions to perform an MRI and a PC-MRI in 2D images. Since it is meant to work as an introductory tool, many assumptions are made in order to simplify its usage. The most important ones are:

- On-resonance hypothesis.
- RF-pulse is done instantaneously.
- The gradients used to construct GRE sequences change their amplitude instantaneously.
- Absence of inhomogeneities.

Under those assumptions, the equations behind MRI are solved like in the previous chapter.
When trying to reconstruct an image, the signal will be stored in a $N_y \times N_x$ matrix, where N_y corresponds to the total number of phase encoding steps and N_x are the total of frequency encoding steps applied during a single readout of the signal. When thinking in terms of spatial frequencies in the k-space, N_y is the number of different k_y and N_x is all the different k_x. Although it is not necessary, the signal matrix is chosen to be the same size that the image to reconstruct, being:

$$\begin{aligned} S_P(q_x, q_y) &= \sum_{p_x=0}^{N_x-1} \sum_{p_y=0}^{N_y-1} e^{-\frac{t(q_x)-t_0}{T_2}} \rho_P(p_x, p_y) e^{-i(\phi(p_x,p_y,q_x,q_y)-\phi_0)} \\ &\forall (q_x, q_y) \in N_x \times N_y \end{aligned} \tag{3.1}$$

Where $\rho_P(p_x, p_y)$ represents the exact proton density of the image, $t(q_x)$ indicates the time of acquisition of the point q_x and t_0 is the start of the sequence once the RF-pulse is done.
To keep it simple the Python solver only creates raster-like Cartesian GRE sequences. Since it is a uniformly spaced Cartesian k-space, the image reconstruction is done using the inverse fast Fourier transform algorithm which is already implemented in the NumPy library. It goes as follows:

1) **Creation of the first GRE sequence to be played**: As a convention, the first sequence starts from the line that contains $k_{y,max}$, it will be changed during the filling of the k-space.
2) **Obtaining the signal**: Creation and filling of the signal matrix according to (3.1).
3) **Reconstructing the image**: Performing an inverse fast Fourier transform on the signal matrix previously filled.

4) **Performing a PC-MRI** *(Optional)*: If steps 1) to 3) are followed for two GRE sequences that were constructed accordingly to what was said in *Section 2.2*, then it is possible to perform a PC-MRI.

The image to reconstruct is the Shepp-Logan phantom [21], shown in *Figure 3.1*, which is a standard test image used in MRI and simulates a human head. For our test, the image size, also known as Field-of-View (FOV) is of

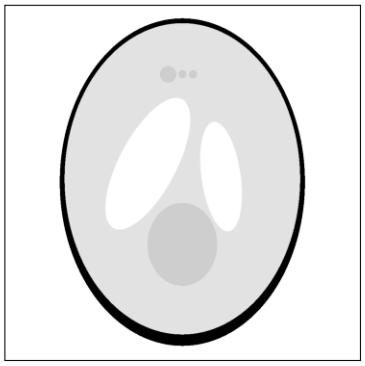

Figure 3.1: *Shepp-Logan phantom. It simulates a human head. With the exterior contour being the skull, the two big ellipses simulating the ventricles, the smaller ellipses and the circle being tumors and the rest is the gray matter [21]. To give a sense to the PC-MRI, we will treat the circle as a vein so we can study the blood flow velocity.*

256×256 mm^2 , and it has a resolution, which here means our pixel size, of 1×1 mm^2 . Resulting in an image matrix of 256×256.
As for the PC-MRI, the grey circle between the who ellipses of the phantom acts as a vein where a Poiseuille flow that goes along the z-direction (e.g. normal to the image since it's a 2D image on the xy-plane) represents the blood flow, with no velocities or whatsoever on any other direction. A visualization of the simulation is shown in *Figure 3.2*. To make the first GRE sequence, a repetition time T_R, which just defines the duration of a single acquisition when doing an MRI, must be given. Here it is $TR = 0.006$ s. Secondly, the addition of gradients in the sequence, it has a prephasing and readout gradient along a flow compensating gradient in the x-direction, to perform the frequency encoding of the signal. Before the readout gradient

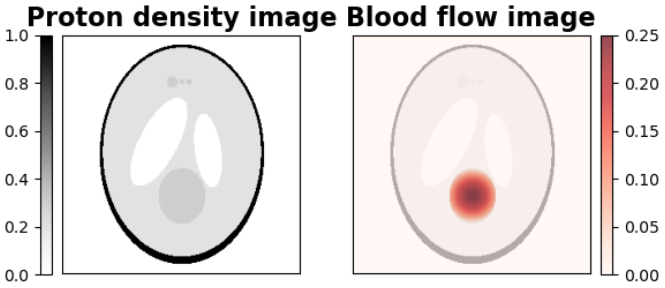

Figure 3.2: *On the right, a proton density image of the Shepp-Logan phantom and on the left, a magnitude image of the z-component for the blood flow.*

(which is the gradient that is played when acquiring the signal) a phase encoding gradient is added in the y-direction.
To perform a PC-MRI, a second sequence almost exact to the first one but with a bipolar gradient in the z-direction is also made. The GRE sequences for a single T_R look like the ones in *Figure 3.3*.

As for the PC-MRI, a previous knowledge of the type of flow is required, here it is perfectly known, and thus, we can accurately define a velocity encoding parameter that minimizes the errors that might appear. For that, and knowing that the maximum velocity that the z-component can achieve is of 25 mm/s, $V_{ENC} = (0.3, 0.3, 0.3)^T$. The results can be seen in *Figure 3.4*, and we have also added a line comparison to better observe the differences in *Figure 3.5*.

The reconstructed proton density is almost exactly the same, the difference is because of the relaxation factor $e^{-\frac{t(q_x)-t_0}{T_2}}$. If not for this factor, both images would be identical. As for the PC-MRI, although the original blood flow is reconstructed correctly, some errors appear. It is still unclear why it happens, a plausible explanation could be that when performing the PC-MRI some zones carry a numerical error due to not being exactly zero and that is reflected in the final reconstruction.

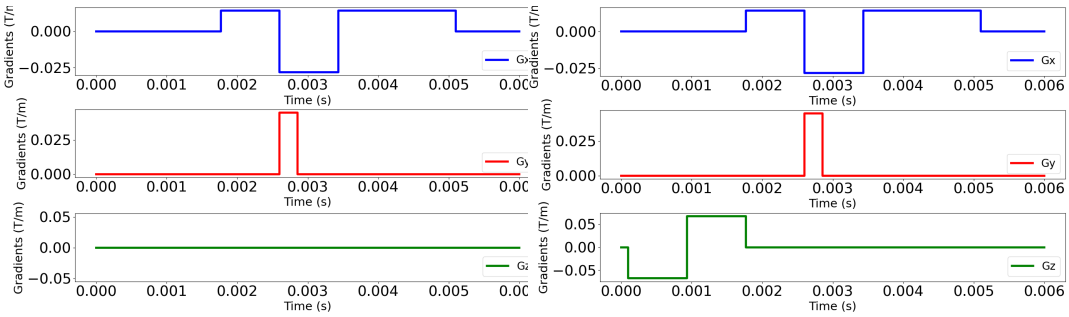

(a) *GRE sequence of reference* (b) *GRE sequence for the PC-MRI*

Figure 3.3: *GRE sequences created with the Python solver. Each line correspond to one direction, the blue is the x-direction, the red is the y-direction and the green is the z-direction. The first one is used as a reference and is enough for an MRI. The second one is the one that is created when the objective is to perform a PC-MRI. It is the same as the one on the left except for the gradient that is added alongside the velocity encoding direction (the green one in that case).*

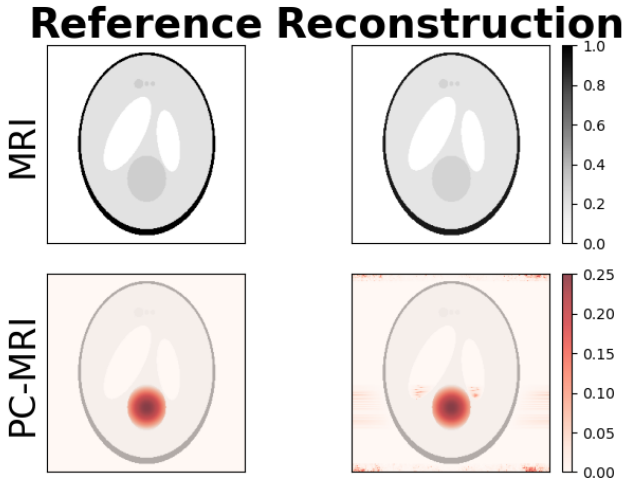

Figure 3.4: *Comparison between the original proton density and blood flow and the reconstruction obtained when performing an MRI and a PC-MRI.*

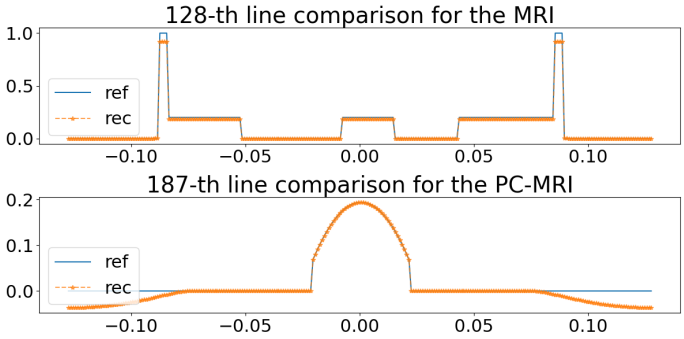

Figure 3.5: *Line comparison between the original proton density and blood flow and the reconstruction obtained when performing an MRI and a PC-MRI.*

3.3 Obtaining a sequence from a trajectory

The introduction of spatial frequencies, as an addition to help to understand the signal as a Fourier transform of the proton density, can also help to visualize the fact that playing a GRE sequence can be seen as moving through the space of spatial frequencies, commonly known as k-space. This displacement done during a sequence is known as a trajectory. In *Figure 3.6* there is defined a simple GRE sequence used to do an MRI. When describing it as a trajectory in the k-space, the step by step evolution of such trajectory is described in *Figure 3.7*.
The first image in *Figure 3.7* corresponds to the start of the trajectory, no gradient has been played yet so it is in the center. Once the phase-encoding gradient is over, it correspond to a displacement along the k_y-direction in the k-space, as it is shown in the second image. The the third image shows the position of the trajectory once the prephasing gradient has ended, since it is a negative gradient in the x-direction, it corresponds to a negative displacement in the k_x-direction in the k-space. Finally the readout gradient is played, many more points appear here since they correspond to the points in the k-space that are being sampled for the MRI. Since it is a positive gradient in the x-direction, the displacement occurs to the right in the k_x-direction in the k-space.
It has been noted that observing the trajectories on the k-space that a sequence makes could be an interesting way to study the properties of that sequence [19] [20].

With this example it becomes clear that a trajectory can be extracted from a sequence, but the inverse can also be done, and this section consists of an explanation of a sequence can be created from a trajectory.

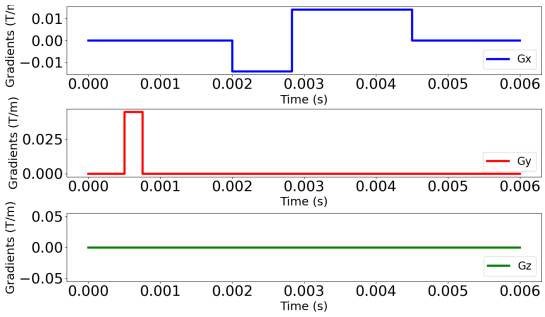

Figure 3.6: *Basic GRE sequence that can be used for MRI, it only has the gradients to spatially encode the 2D signal. The phase-encoding gradient in the y-direction, and the prephasing and readout gradient in the x-direction, which are the first and the second one respectively.*

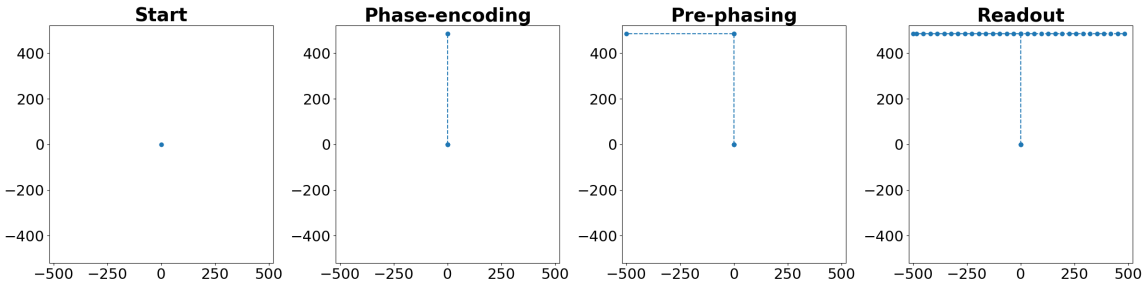

Figure 3.7: *Evolution of the trajectory following the sequence in Figure 3.6.*

3.3.1 Theory

Due to the huge amount of trajectories that can be found outside of the most used methods, a general way to obtain a GRE sequence that can be played to perform an MRI in the Python solver is shown and explained here.
A spatial frequency is defined as k:

$$k(t) = \frac{\gamma}{2\pi} \int_{t_0}^{t} G(t')dt' \tag{3.2}$$

Where γ denotes the gyromagnetic ratio, $t_0 \in \mathbb{R}_+$ is the starting time of the sequence and $G(t)$ is the gradient strength function.
From (3.2), $G(t)$ is the derivative in time of $k(t)$ and thus:

$$k'(t) = \frac{\gamma}{2\pi} G(t), \ \forall t \in]0, TR[\tag{3.3}$$

A Taylor series expansion can be used in order to get an expression for k' from k, for an arbitrary point displacement $\Delta t > 0$ such that $t + \Delta t \in]0, TR[$ gives:

$$\begin{aligned} k(t + \Delta t) &= k(t) + \Delta t k'(t) + \mathcal{O}(|\Delta t|^2) \\ k'(t) &= \frac{k(t + \Delta t) - k(t)}{\Delta t} + \mathcal{O}(|\Delta t|) \\ k'(t) &\simeq \frac{k(t + \Delta t) - k(t)}{\Delta t} \end{aligned} \tag{3.4}$$

Combining equations (3.3) and (3.4):

$$G(t) \simeq \frac{2\pi}{\gamma} \frac{k(t + \Delta t) - k(t)}{\Delta t} \tag{3.5}$$

To discretize (3.5) it is needed a vector of spatial frequencies $K = [k_0, k_1, ..., k_{n-1}, k_n] \in \mathbb{R}^n$. With every one of its components defined as $k_i = k(t_i), \ \forall i \in \{0, ..., n\}$, with $t_i \in [0, TR], \ \forall i \in \{0, ..., n\}$ such that
$0 = t_0 < t_1 < ... < t_{n-1} < t_n = TR$. It is assumed that $k_0 = k(0) = k(t_0) = 0$ and $k_n = k(TR) = k(t_n) = k(t_{n-1})$, which are fair assumptions since the trajectory always starts at the center of the k-space during each repetition time and once the signal is acquired during a TR, there is no need to keep applying a gradient field. Which means that the spatial frequency

stays at the same place between the last signal acquisition and the TR. Using the expression (3.5) with the discretized values gives a vector of values $G_{VECT} = [G_0, G_1, ..., G_{n-1}, G_n]$ defined as:

$$G_i = \begin{cases} G_0 = G_n = 0, & if\ i = \{0, n\} \\ G_i = \frac{2\pi}{\gamma} \frac{k_{i+1} - k_i}{t_{i+1} - t_i}, & if\ i \in \{1, ..., n-1\} \end{cases}$$

The constrains in G_0 and G_n arise from the assumptions made on k_0 and k_n. The convergence ratio of the scheme (which is of order 1) can be improved by choosing to implement a more complex finite difference scheme. $G_i \simeq G(t_i)$ is an approximation of the gradient strength function at time t_i.
It is important to remark that in order for this method to work, each point k_i must be assigned a time t_i, this can be done manually to precisely control the sequence that is obtained.

3.3.2 Examples

Firstly, to verify that the method to generate sequences from trajectories presented above works, a comparison between a GRE sequence generated in the Python solver and a GRE sequence that has been created from the trajectory issued of the first sequence is made. Both trajectories should be identical and when doing an MRI with them, the result should be the same. The results of such comparison are shown in *Figure 3.8*, both raster-like Cartesian GRE sequence are exactly the same so it is expected for both to work when doing an MRI.
Secondly, since the main motivation of reconstructing GRE sequences from trajectories was to have a quick way of working with different trajectories when doing MRI simulations in the Python solver, a radial trajectory is constructed. And then a GRE sequence is generated for each acquisition line of the radial trajectory. *Figure 3.9* shows what a single line of a radial trajectory and its associated GRE sequence should look like.

Figure 3.10 shows the reconstructions that are obtained from each sequence alongside the reference. In *Figure 3.11* there is a line comparison of said reconstructions to better observe their accuracy. For both Cartesian sequences, the one where the gradients were generated in the Python solver and the one where the gradients where reconstructed directly from trajectories, the result is the same, as expected.

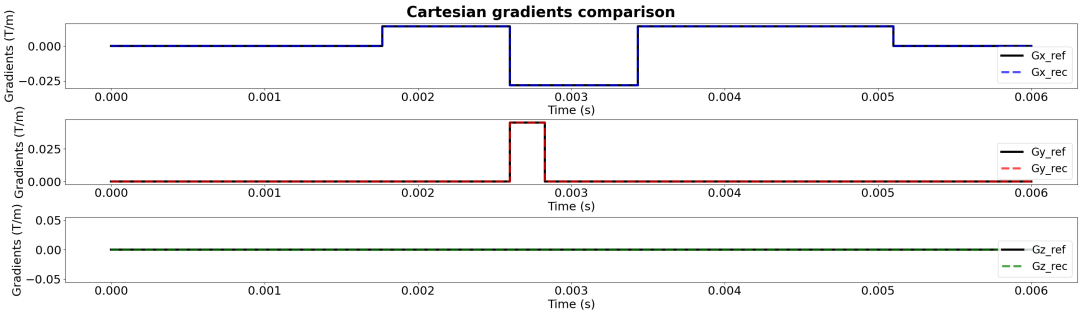

Figure 3.8: *Figure where the reference GRE sequence (in black) and the GRE sequence (dashed line) generated from the trajectory described by the first GRE sequence, they match perfectly in the image.*

The image reconstructed from the radial trajectory is not as good, this is due to how radial trajectories work, with higher density of data points in the center of the k-space, allowing for a better reconstruction of the general shape. But with a lower density of data points in the exterior of the k-space (e.g. the high frequencies) making it harder to have contrast in the image. *Figure 3.10* shows this, allowing us to discern the shape of the object reconstructed, but without clear edges unlike the others.

Despite all that it is indeed possible to make sequences from trajectories, and they can be used to perform an MRI. As previously commented, this can be helpful when studying the benefits of certain trajectories when doing simulations, while allowing someone to test them quickly without needing to implement them by hand every time.

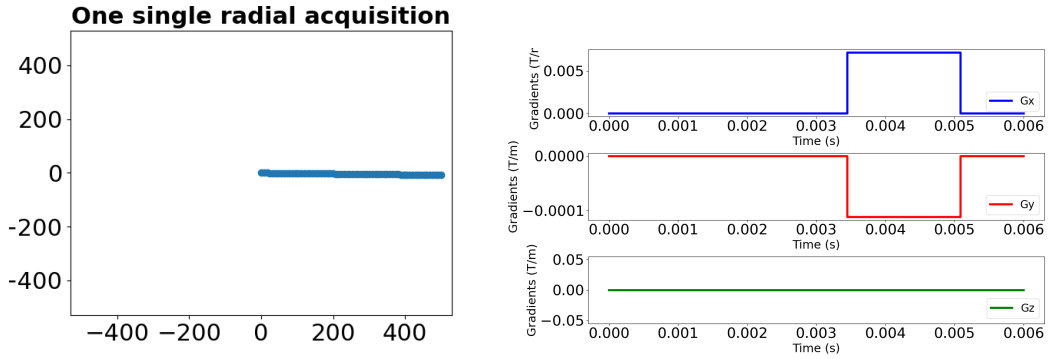

(a) *Radial trajectory from which get the GRE sequence is obtained*

(b) *GRE sequence obtained from this trajectory*

Figure 3.9: *GRE sequence that generated from a radial trajectory*

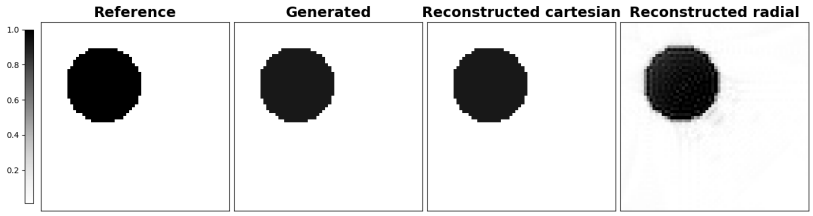

Figure 3.10: *Images obtained for each sequence*

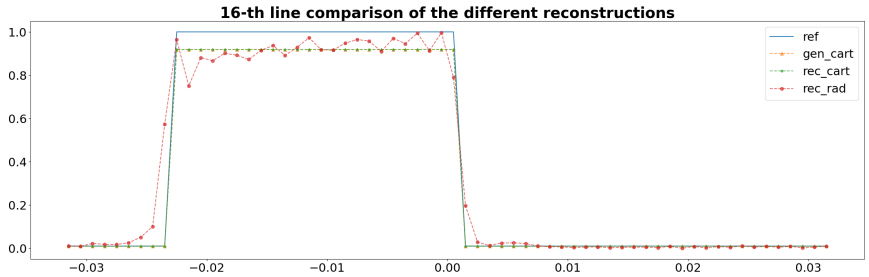

Figure 3.11: *Line comparison of the images*

3.4 Radial trajectories for motion correction

The most used trajectory in the clinic is the raster-like Cartesian trajectory. Where, in 2D for example, the k-space is divided by a Cartesian grid, and the signal is collected on those points in the Cartesian grid by first getting to its appropriate "height" k_y (which was previously defined as phase-encoding) and then acquiring all the points of the Cartesian grid on that height. This is the classical method and within its advantages there is the direct reconstruction of an image by an inverse fast Fourier transform, its robustness to certain artifacts in comparison to other methods, a lot of techniques have been invented in order to solve some of the problems that appear when using it, etc.
On the other hand, there are virtually an infinity of different non-Cartesian trajectories to study, many of them might not propose any advantage over the classical approach, but others might. Between those trajectories of interest, one that has been gaining attention due to its performance under certain circumstance in comparison with the Cartesian ones, is the radial trajectory. When performing an acquisition using a Cartesian trajectory, not every acquisition contains the same information about the object that is being imaged. Some acquisitions might have been done entirely on the border of the k-space while only a few contain information of the center. This is not the case when performing a radial acquisition, each acquisition contains the same amount of information on the k-space, for certain situations this might be beneficial. One of those cases where a radial acquisition arises as a better option over the Cartesian one is when it is necessary to mitigate the artifacts that are caused due to motion during an MRI.
Motion artifacts are a major issue in medical imaging, specially for MRI, since due to its inherently long acquisition time, they are more propense to happen, and if strong enough, might render the image unusable. The problem have been approached in different ways [22], ideally, the patient should not move, but sometimes this is just not possible. Other approaches involve the use of different trajectories more robust to movement, such as PROPELLER [23] or, as mentioned before, a radial sequence.

3.4.1 Theory

In order to detect and correct translation the 2D version of the Fourier slice theorem is used, which states that a 1D slice that passes through the origin

of the 2D Fourier transform of the image, is the Fourier pair of the projection of the image to a 1D line that is parallel to our slice, *Figure 3.12* shows a visual explanation of the theorem. And so, if a projection of the object is

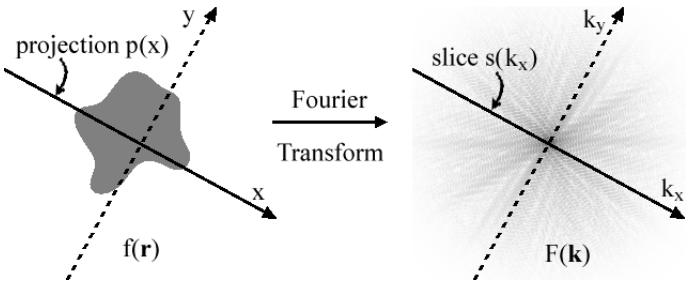

Figure 3.12: *Scheme to illustrate the Fourier slice theorem, the projection $p(x)$ of a 2D function $f(\mathbf{r})$ has as Fourier transform the slice $s(k_x)$ with the same direction as the projection of the 2D Fourier transform $F(\mathbf{k})$ of the 2D function*

done in the same direction of the movement, it will appear also as a translation in the projection, as shown in *Figure 3.13*. Thanks to the Fourier slice theorem, if two slices parallel to those projections and passing trough the center were extracted, (here would mean taking the k_x axis since the projection were done on the x axis) the same translation would be seen when reconstructing said projections. So with minimal information the movement can be detected and corrected.
A control sequence (also known as a navigator) [24], which is a sequence that will be played regularly, is used. It is always the same, so it corresponds to the same trajectory in the k-space (here it is the same as a slice) and with those the control sequences the projection of the image over said line is reconstructed, if there is movement it will be detected it. With this information the data that was affected by such movement can be corrected. It is important to note that in order to do so it is required a previous knowledge of the movement, in particular its direction.
Another important remark to be made is that by using this method, the advantages of the radial sampling over the Cartesian become evident. Firstly, there is only one type of control sequence that can be used on the Cartesian sampling, and that is the one that corresponds to the k_x line, so the only movement that can be detected is the one that happens on the x-direction, as shown in *Figure 3.14*. While in radial, you can define your control sequence in any direction on the 2D plane.

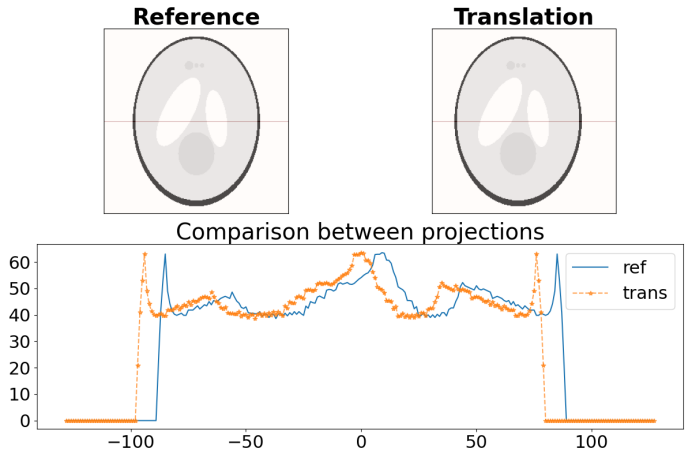

Figure 3.13: *Example of how the translation of an object affects the projection done on a line parallel to the direction of such translation, here the object is moved 9 pixels to the left, and the projection (which is done on the red line) has also moved 9 pixels to the left.*

As a remark, only the effect that a translation of the object during an MRI is being studied, there are obviously other movements that can cause artifacts when reconstructing an image. Rotations and expansions/contractions are other sources of motion artifacts. Both of those type of movements can also be corrected when using radial trajectories to fill the k-space. For rotations, navigators have been developed to detect them and correct them too [25], and which combined with translations on a 3D object, the most common one is known as the *cloverleaf navigator* [26].
When trying to address artifacts issued from the expansion/contraction of the object, radial trajectories also present a clear solution, since the amplitude of the center of the k-space, which is sampled for each trajectory, can be compared. The trajectories that have been corrupted by that movement are detected and corrected.

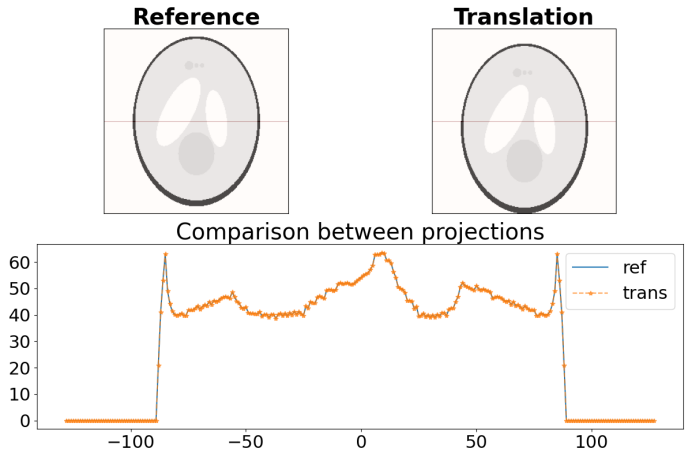

Figure 3.14: *Here the movement is done over the y-axis but the projection is done on the x-axis, there is no difference between the projections (done on the red line), so it is not possible the detect movement from this projection.*

3.4.2 Example

To do this test-case, the Python package SigPy is used [27], it is designed to perform high performance iterative reconstruction and common MRI reconstruction methods and functions are already implemented there.
The movement happens during the whole acquisition time but it is assumed that the object remains in its place during the acquisition of each line. As an addition, it is also supposed that the patient is making an effort to stay still, and so it is not a continuous movement that happens gradually, but more like a sudden movement that happens at a certain time and then it stayed there for a while before moving again. Finally, assume that the movement happens always in the same direction and that such direction is known.
As our acquisition technique, a golden angle radial acquisition will be used, which has become the standard when doing radial sequences due to its advantages over a normal radial acquisition. In a golden angle radial acquisition, the angle difference between each acquisition is given by the golden ration.
In *Figure 3.15* the different position that the object will have during the MRI are shown.

As indicates the red line, this movement follows the direction of the line $\mathcal{L} = \{(x, y) \in \mathbb{R}^2 | y = -x\}$, and so the slice in the k-space must have the

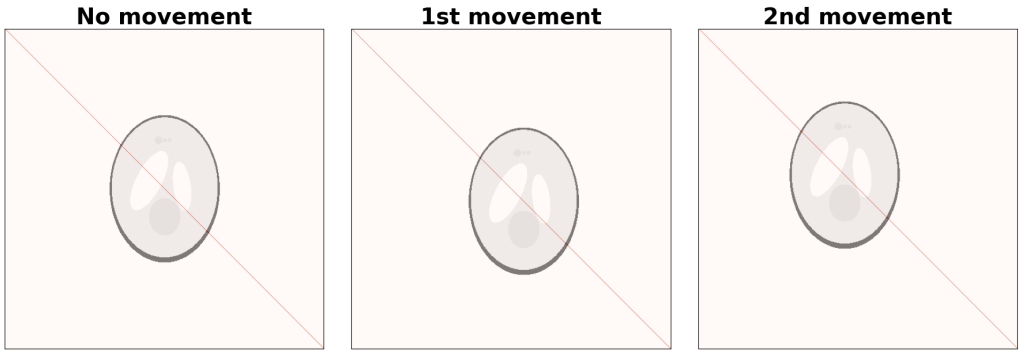

Figure 3.15: *Illustration of the movements that will corrupt the data acquired during the MRI, the first third is done with the object staying in place, the second third is done with the object being moved 20 pixels to the left and down with respect to the origin, and in the last the object is displaced 22 pixels to the right and up with respect to the origin.*

same direction. It follows naturally to define the control sequence as shown in *Figure 3.16*.

The control sequence will be played every 13 acquisitions, and so it acts as

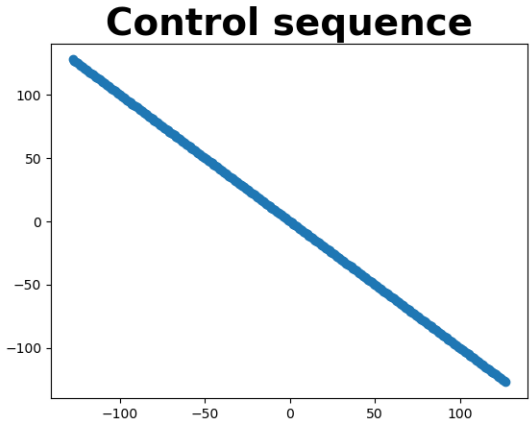

Figure 3.16: *Control sequence used to detect the movement and correct it.*

an indicator of the position of the object for the 13 acquisitions that follow the control sequence. With that, in *Figure 3.17* there is a comparison of the reconstructed image with and without the motion correction.

Without correction, as shown in *Figure 3.17*, the object is repeated in the

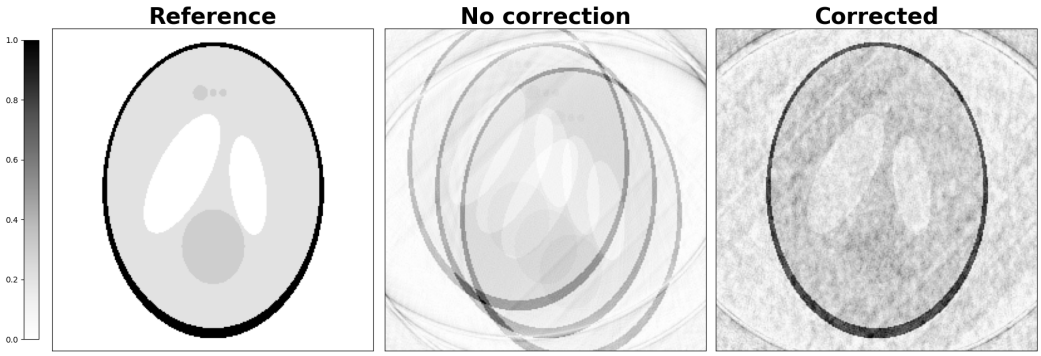

Figure 3.17: *Comparison of the image reconstructed with and without motion correction, without motion correction the object appears on the other positions that it has been measured, while with motion correction those apparitions disappear, giving a more clear image.*

three distinct positions that it was measured. It is expected from a radial trajectory since each acquisition time contains the same amount of information and it was measured almost the same amount of acquisitions in each position, so it is natural for the image to look like that. When looking at the image with the motion correction applied, the repeated images disappeared but the new image is not as good. The general shape is properly reconstructed and when there is a high contrast between the objects (such as in the skull or the ventricles with the gray matter) those are still observable in the image. But the tumors become much more difficult to find.

Chapter 4

Discussion and moving forward

4.1 Discussion

As already mentioned at the beginning this report is meant to act as an introduction to the theory behind MRI. As such the test-cases showed here are simplifications that aim to showcase some properties of MRI and problems that one might find when doing it, and the techniques that might be used to address such problems. As it has already been said, MRI is complex, and some of the problems that were found when doing the test cases might be caused due to my own lack of deep understanding of the subject, such as the apparition of extra dephasing with its consequent velocity that should not be here, or the difficulties when reconstructing more complex images as the Shepp-Logan phantom with radial trajectories.

4.2 Moving forward

The idea of this internship to gain a proper understanding on what is being done here at the IMAG on the subject of *in silico* MRI. To do so, it is important to know how an MRI works and to learn to use the Yales2BIO solver, which is used to perform such technique. So the idea is to continue to keep studying the techniques that can be used alongside radial trajectories in order to encode movement/flow information to preform an MRI or PC-MRI, and gain more practice with the solver. Once the internship is over, it will be followed with a thesis financed by the ANR under the supervision of Monica Sigovan, a research scientist working at CREATIS in Lyon.

Bibliography

[1] P. C. Lauterbur. "Image formation by induced local interactions: Examples employing nuclear magnetic resonance". In: *Nature* (1973).

[2] Frank Gaillard. *Normal brain (MRI), case study.* https://radiopaedia.org/cases/37605. Accessed: 24 June 2025. 2015.

[3] Lam Van Le. *Segond fracture, case study.* https://radiopaedia.org/cases/207562. Accessed: 24 June 2025. 2025.

[4] Yanchun Zhu et al. "Review: K-space trajectory development". In: *2013 IEEE International Conference on Medical Imaging Physics and Engineering*. 2013, pp. 356–360. DOI: 10.1109/ICMIPE.2013.6864568.

[5] Li Feng. "Golden-Angle Radial MRI: Basics, Advances, and Applications". In: *Journal of Magnetic Resonance Imaging* 56.1 (2022), pp. 45–62. DOI: https://doi.org/10.1002/jmri.28187. eprint: https://onlinelibrary.wiley.com/doi/pdf/10.1002/jmri.28187. URL: https://onlinelibrary.wiley.com/doi/abs/10.1002/jmri.28187.

[6] Charles A. Mistretta. "Undersampled radial MR acquisition and highly constrained back projection (HYPR) reconstruction: Potential medical imaging applications in the post-Nyquist era". In: *Journal of Magnetic Resonance Imaging* 29.3 (2009), pp. 501–516. DOI: https://doi.org/10.1002/jmri.21683. eprint: https://onlinelibrary.wiley.com/doi/pdf/10.1002/jmri.21683. URL: https://onlinelibrary.wiley.com/doi/abs/10.1002/jmri.21683.

[7] Huimin Wu et al. "Noncontrast-enhanced three-dimensional (3D) intracranial MR angiography using pseudocontinuous arterial spin labeling and accelerated 3D radial acquisition". In: *Magnetic Resonance in Medicine* 69.3 (2013), pp. 708–715. DOI: https://doi.org/10.1002/

mrm.24298. eprint: https://onlinelibrary.wiley.com/doi/pdf/10.1002/mrm.24298. URL: https://onlinelibrary.wiley.com/doi/abs/10.1002/mrm.24298.

[8] Hassan Haji-Valizadeh et al. "Highly accelerated, real-time phase-contrast MRI using radial k-space sampling and GROG-GRASP reconstruction: a feasibility study in pediatric patients with congenital heart disease". In: *NMR in Biomedicine* 33.5 (2020). e4240 NBM-19-0205.R2, e4240. DOI: https://doi.org/10.1002/nbm.4240. eprint: https://analyticalsciencejournals.onlinelibrary.wiley.com/doi/pdf/10.1002/nbm.4240. URL: https://analyticalsciencejournals.onlinelibrary.wiley.com/doi/abs/10.1002/nbm.4240.

[9] Özkan Özsarlak et al. "MR angiography of the intracranial vessels: Technical aspects and clinical applications". In: *Neuroradiology* 46 (Jan. 2005), pp. 955–72. DOI: 10.1007/s00234-004-1297-9.

[10] Stephanie Func, Aylin Demir, and Jeanette Schulz-Menger. "Clinical usefulness of 4D flow in adult cardiovascular MRI". In: *MAGNETOM Flash* 72 (2019), pp. 48–52.

[11] Thomas Puiseux. "Numerical simulations for phase-contrast magnetic resonance imaging". Theses. Université Montpellier, Nov. 2019. URL: https://theses.hal.science/tel-02934286.

[12] Morgane Garreau. "Simulations hémodynamiques pour l'IRM : contrôle qualité, optimisation et intégration à la pratique clinique". Theses. Université de Montpellier, Nov. 2023. URL: https://theses.hal.science/tel-04552933.

[13] Thomas Puiseux et al. "Numerical simulation of time-resolved 3D phase-contrast magnetic resonance imaging". In: *PLoS One* (2021).

[14] J. Sigueenza et al. "YALES2BIO: A Computational Fluid Dynamics Software Dedicated to the Prediction of Blood Flows in Biomedical Devices". In: *5th International Conference on Biomedical Engineering in Vietnam*. Ed. by VanToi et al. Vol. 46. WOS:000357778100002. 2015, pp. 7–10. URL: https://hal.science/hal-01612345.

[15] I. I. Rabi et al. "A New Method of Measuring Nuclear Magnetic Moment". In: *Phys. Rev.* 53 (4 Feb. 1938), pp. 318–318. DOI: 10.1103/PhysRev.53.318. URL: https://link.aps.org/doi/10.1103/PhysRev.53.318.

[16] Abi Berger. "Magnetic resonance imaging". In: *BMJ* 324.7328 (2002), p. 35. ISSN: 0959-8138. DOI: 10.1136/bmj.324.7328.35. eprint: https://www.bmj.com/content/324/7328/35.full.pdf. URL: https://www.bmj.com/content/324/7328/35.

[17] Matt A. Bernstein, Kevin F. King, and Xiaohong Joe Zhou. *Handbook of MRI Pulse Sequences*. English (US). Publisher Copyright: © 2004 Elsevier Inc. All rights reserved. Elsevier Inc., Sept. 2004. ISBN: 9780120928613. DOI: 10.1016/B978-0-12-092861-3.X5000-6.

[18] F. Bloch. "Nuclear Induction". In: *Phys. Rev.* 70 (7-8 Oct. 1946), pp. 460–474. DOI: 10.1103/PhysRev.70.460. URL: https://link.aps.org/doi/10.1103/PhysRev.70.460.

[19] Stig Ljunggren. "A simple graphical representation of fourier-based imaging methods". In: *Journal of Magnetic Resonance (1969)* 54.2 (1983), pp. 338–343. ISSN: 0022-2364. DOI: https://doi.org/10.1016/0022-2364(83)90060-4. URL: https://www.sciencedirect.com/science/article/pii/0022236483900604.

[20] Donald B. Twieg. "The k-trajectory formulation of the NMR imaging process with applications in analysis and synthesis of imaging methods". In: *Medical Physics* 10.5 (1983), pp. 610–621. DOI: https://doi.org/10.1118/1.595331. eprint: https://aapm.onlinelibrary.wiley.com/doi/pdf/10.1118/1.595331. URL: https://aapm.onlinelibrary.wiley.com/doi/abs/10.1118/1.595331.

[21] L. A. Shepp and B. F. Logan. "The Fourier reconstruction of a head section". In: *IEEE Transactions on Nuclear Science* 21.3 (1974), pp. 21–43. DOI: 10.1109/TNS.1974.6499235.

[22] Maxim Zaitsev, Julian Maclaren, and Michael Herbst. "Motion Artefacts in MRI: a Complex Problem with Many Partial Solutions". In: *Journal of magnetic resonance imaging : JMRI* 42 (Jan. 2015). DOI: 10.1002/jmri.24850.

[23] L. A. Pipe. "Motion correction with PROPELLER MRI: application to head motion and free-breathing cardiac imaging." In: *Magnetic resonance in medicine* (1999).

[24] R L Ehman and J P Felmlee. "Adaptive technique for high-definition MR imaging of moving structures." In: *Radiology* 173.1 (1989). PMID: 2781017, pp. 255–263. DOI: 10.1148/radiology.173.1.2781017. eprint: https://doi.org/10.1148/radiology.173.1.2781017. URL: https://doi.org/10.1148/radiology.173.1.2781017.

[25] Zhuo Wu Fu et al. "Orbital navigator echoes for motion measurements in magnetic resonance imaging". In: *Magnetic Resonance in Medicine* 34.5 (1995), pp. 746–753. DOI: https://doi.org/10.1002/mrm.1910340514. eprint: https://onlinelibrary.wiley.com/doi/pdf/10.1002/mrm.1910340514. URL: https://onlinelibrary.wiley.com/doi/abs/10.1002/mrm.1910340514.

[26] André J.W. van der Kouwe, Thomas Benner, and Anders M. Dale. "Real-time rigid body motion correction and shimming using cloverleaf navigators". In: *Magnetic Resonance in Medicine* 56.5 (2006), pp. 1019–1032. DOI: https://doi.org/10.1002/mrm.21038. eprint: https://onlinelibrary.wiley.com/doi/pdf/10.1002/mrm.21038. URL: https://onlinelibrary.wiley.com/doi/abs/10.1002/mrm.21038.

[27] Franck Ong and Michael Lustig. "SigPy: a python package for high performance iterative reconstruction". In: *Proceedings of the ISMRM 27th Annual Meeting*. Vol. 4819. Montreal, Quebec, Canada, 2019.